

Article

PdAg/C Electrocatalysts Synthesized by Thermal Decomposition of Polymeric Precursors Improve Catalytic Activity for Ethanol Oxidation Reaction

Yonis Fornazier Filho ¹, Ana Caroliny Carvalho da Cruz ¹, Rolando Pedicini ² , José Ricardo Cezar Salgado ³ , Rodrigo Vieira Rodrigues ⁴, Priscilla Paiva Luz ¹ , Sergi Garcia-Segura ^{5,*}  and Josimar Ribeiro ^{1,*} 

¹ Centro de Ciências Exatas, Departamento de Química, Universidade Federal do Espírito Santo (UFES), Av. Fernando Ferrari, 514, Vitória 29075-910, Brazil; yonis.fornazier@tutor.ufes.br (Y.F.F.); anacaroliny_c@hotmail.com (A.C.C.d.C.); priscilla.luz@ufes.br (P.P.L.)

² National Research Council, Institute for Advanced Energy Technologies “Nicola Giordano” (CNR-ITAE), Via Santa Lucia Sopra Contesse, 5, 98126 Messina, Italy; rolando.pedicini@itaec.cnr.it

³ Instituto Latino Americano de Ciências da Vida e da Natureza, Universidade Federal da Integração Latino-Americana (UNILA), Foz do Iguaçu 85866-000, Brazil; jose.salgado@unila.edu.br

⁴ Instituto de Química, Universidade de São Paulo (USP), Av. Lineu Prestes, São Paulo 05508-000, Brazil; rodv16429@usp.br

⁵ Nanosystems Engineering Research Center for Nanotechnology-Enabled Water Treatment, School of Sustainable Engineering and the Built Environment, Arizona State University, Tempe, AZ 85287, USA

* Correspondence: sgarcias@asu.edu (S.G.-S.); josimar.ribeiro@ufes.br (J.R.); Tel.: +55-27-40097948 (J.R.)



Citation: Fornazier Filho, Y.; da Cruz, A.C.C.; Pedicini, R.; Salgado, J.R.C.; Rodrigues, R.V.; Luz, P.P.; Garcia-Segura, S.; Ribeiro, J. PdAg/C Electrocatalysts Synthesized by Thermal Decomposition of Polymeric Precursors Improve Catalytic Activity for Ethanol Oxidation Reaction. *Catalysts* **2022**, *12*, 96. <https://doi.org/10.3390/catal12010096>

Academic Editors: David Sebastián, Vincenzo Baglio, Minhua Shao, Carlo Santoro and Yingze Song

Received: 21 December 2021

Accepted: 12 January 2022

Published: 14 January 2022

Publisher's Note: MDPI stays neutral with regard to jurisdictional claims in published maps and institutional affiliations.



Copyright: © 2022 by the authors. Licensee MDPI, Basel, Switzerland. This article is an open access article distributed under the terms and conditions of the Creative Commons Attribution (CC BY) license (<https://creativecommons.org/licenses/by/4.0/>).

Abstract: An efficient ethanol oxidation reaction (EOR) is required to enhance energy production in alcohol-based fuel cells. The use of bimetallic catalysts promises decreasing reliance on platinum group metal (PGM) electrocatalysts by minimizing the use of these expensive materials in the overall electrocatalyst composition. In this article, an alternative method of bimetallic electrocatalyst synthesis based on the use of polymeric precursors is explored. PdAg/C electrocatalysts were synthesized by thermal decomposition of polymeric precursors and used as the anode electrocatalyst for EOR. Different compositions, including pristine Pd/C and Ag/C, as well as bimetallic Pd₈₀Ag₂₀/C, and Pd₆₀Ag₄₀/C electrocatalysts, were evaluated. Synthesized catalysts were characterized, and electrochemical activity evaluated. X-ray diffraction showed a notable change at diffraction peak values for Pd₈₀Ag₂₀/C and Pd₆₀Ag₄₀/C electrocatalysts, suggesting alloying (solid solution) and smaller crystallite sizes for Pd₆₀Ag₄₀/C. In a thermogravimetric analysis, the electrocatalyst Pd₆₀Ag₄₀/C presented changes in the profile of the curves compared to the other electrocatalysts. In the cyclic voltammetry results for EOR in alkaline medium, Pd₆₀Ag₄₀/C presented a more negative onset potential, a higher current density at the oxidation peak, and a larger electrically active area. Chronoamperometry tests indicated a lower poisoning rate for Pd₆₀Ag₄₀/C, a fact also observed in the CO-stripping voltammetry analysis due to its low onset potential. As the best performing electrocatalyst, Pd₆₀Ag₄₀/C has a lower mass of Pd (a noble and expensive metal) in its composition. It can be inferred that this bimetallic composition can contribute to decreasing the amount of Pd required while increasing the fuel cell performance and expected life. PdAg-type electrocatalysts can provide an economically feasible alternative to pure PGM-electrocatalysts for use as the anode in EOR in fuel cells.

Keywords: alkaline direct ethanol fuel cell; electrocatalysts; ethanol oxidation; PdAg/C; performance with the economy

1. Introduction

Bimetallic nanostructures can benefit from synergistic effects at the nanoscale that result in enhanced performance when compared with pristine monometallic structures [1].

An important application of these nanostructures in the energy nexus is the oxidation reaction of low molecular weight alcohols in fuel cells, such as methanol, ethanol, and ethylene glycol. Electrochemical oxidation of alcohols has been highlighted as an alternative to replace hydrogen because, despite hydrogen showing high-power densities, it is difficult to transport and store [2]. Ethanol is an alcohol produced from renewable sources, non-toxic, and produces energy with good power densities [2].

Ethanol oxidation can exhibit remarkably high efficiency if it is completely oxidized to CO₂ and H₂O. However, breaking the C-C bond of ethanol is not easy, and complete electrochemical oxidation to CO₂ might be incomplete, yielding CO. Evolution of CO can result in electrocatalyst poisoning and decrease catalytic activity over time [2–6].

Pt and Pt-based bimetallic electrocatalyst nanostructures can activate the ethanol oxidation reaction (EOR) under ambient conditions, but this process generates CO, which strongly combines with Pt, blocking its active sites for the oxidation of new ethanol molecules [5]. In this context, the proposed replacement of Pt with Pd-based electrocatalysts for reactions in the alkaline medium has been found promising to decrease unwanted poisoning, and it has been observed that Pd-based bimetallic electrocatalysts can decrease undesired poisoning and minimize the usage of Pd [1,7–26].

The enhanced electrocatalytic performance exhibited by bimetallic electrocatalysts may be related to several factors, such as particle size, structure, ligands, crystal facets, surface area, and electronic effects [10,16,21,22]. Therefore, elucidating fundamental aspects of novel bimetallic catalysts is essential for the strategic engineering design of electrocatalysts for EOR.

Recent literature reports demonstrate that PdM (where M is a different non-PGM metal) electrocatalyst synthesis methods play an essential role in the electrocatalysts morphology and significantly affect the synergistic catalytic performance [22]. Table 1 presents a brief summary of the synthesis methods most commonly reported in the literature, their basic principles, as well their advantages and disadvantages.

Table 1. Main synthesis methods for Pd-based electrocatalysts.

Method	Principle	Advantages	Disadvantages	References
Impregnation-reduction	Reduction of salts in alkaline pH and ethylene glycol	Low-cost and quick reaction	Difficulty in maintaining pH at ~12	[10]
Modified impregnation (sodium borohydride method)	Impregnation of salts at acid pH and citrate with excess NaBH ₄	Low-cost and fast reaction routes	Harmful to humans and the environment	[16]
Hydrothermal	Reduction and polymerization in the presence of ethylene glycol and citrate at alkaline pH	Low cost, easy to handle materials	Long reaction time and strict temperature control	[17]
Thermal decomposition of polymeric precursors (Pechini method)	Esterification, polymerization, and calcination of percussion salts from ethylene glycol and citric acid	Easy handling, low cost, and insensitivity to the presence of water	Forms large and usually agglomerated particles	[23]
Hydrogen	Reduction of metal salts using hydrogen as reducing agent	Simple, cheap, fast, and clean method	Flammable, explosive, and hydrogen is an expensive and difficult gas to transport.	[24]
Ascorbic acid	Ascorbic acid is used to reduce metal salts at temperatures of 80 °C	Easy application and low toxicity	Sensitive to heat and light	[25]
Polyol	Reduction of metals by poly-alcohols, such as ethylene glycol and subsequent heat treatment	Low-cost and low toxicity	Forms large and agglomerated particles	[26]

Silver (Ag) is an earth-abundant and relatively cheap raw material. The use of chemical salts of Ag to prepare PdAg exhibited good electrochemical results [27,28]. Unlike other PdM electrocatalysts, PdAg is known to form homogeneous solid solutions in all compositions. The formation of homogeneous solid domains can enable alloy formation with integrated bimetallic catalytic sites (similar to single-atom catalysts) which make PdAg catalysts very attractive for electrochemical studies [27,29,30]. Li et al. observed that PdAg/C electrocatalysts prepared by non-electrolytic methods showed electrocatalytic activities and enhanced stability for EOR compared to Pd/C and Ag/C on alkaline medium [31]. Carrera-Cerritos et al. observed a significant improvement in electrocatalytic activity in their studies of PdAg electrocatalysts in EOR [29]. Feng et al. observed that electrochemical results of PdAg alloys for EOR on an alkaline medium showed remarkable improvement due to the physical changes on the Pd structure with the insertion of Ag into the Pd structure [32]. However, the method of preparation can affect the structure and influence performance of the electrocatalyst.

This study explores the preparation of PdAg/C electrocatalysts using a novel method based on the thermal decomposition of polymeric precursors. The thermal decomposition method is an easily scalable process that increases economic feasibility and eases technology translation. Electrocatalysts of Pd₈₀Ag₂₀/C and Pd₆₀Ag₄₀/C were selected as providing representative thresholds of composition that maintain relevant activity associated with Pd catalysts while minimizing the need for platinum group metal bulk materials by including alloyed Ag. This approach can provide a path to reducing the cost of electrocatalyst production.

2. Results and Discussion

2.1. Characterizing the Electrocatalyst

Figure 1 presents the XRD patterns of the synthesized Pd/C, PdAg/C, and Ag/C electrocatalysts. The diffractogram of Pd/C showed characteristic peaks at 2θ of 40.0° , 46.3° , 67.9° , and 85.6° that correspond to the Miller index planes (111), (200), (220), and (222), respectively (JCPDS 05-0681) [10,16]. Interestingly, the pristine Pd electrocatalyst also presented peaks associated with the tetragonal structure of PdO that allowed the inference of a partial Pd oxidation calcination process at 573 K. The characteristic peaks of PdO observed at 2θ of 33.5° , 41.5° , 54.3° , 59.9° , 60.5° , and 81.8° correspond to the planes (101), (110), (112), (103), (220), and (222), respectively (JCPDS 41-1107) [23], presenting 60% peaks of this oxide and consequently a relative proportion of 1.5 in relation to the Pd peaks.

Conversely, the pristine Ag/C electrocatalyst only showed peaks associated with the fcc structure of silver domains with the absence of silver oxide structures. The characteristic peaks of Ag at 37.9° , 43.9° , 63.8° , 76.8° , and 81.1° were associated with the Miller index planes (111), (200), (220), (311), and (222), respectively.

The bimetallic electrocatalysts did not show peaks associated with PdO which indicates a stabilizing effect of Ag. The composition Pd₈₀Ag₂₀/C showed diffraction peaks at 39.9° , 46.4° , 67.6° , and 86.1° corresponding to the Pd planes in fcc structure at (111), (200), (220), and (222) (JCPDS 87-0643), whereas the higher Ag substitution resulted in peak shifting towards low diffraction angles as the Ag atom is smaller than the Pd atom. In consequence, Pd₆₀Ag₄₀/C showed diffraction peaks at 39.4° , 45.8° , 67.1° , and 84.9° corresponding to Pd planes in fcc structure at (111), (200), (220), and (222), respectively (JCPDS 87-0641) [30]. It is important to note that the diffraction peaks observed showed a shift in relation to pristine Pd/C and Ag/C. These results imply the formation of an alloy solution with fcc crystalline structure, as has been previously reported in the literature for PdAg electrocatalysts [20]. Similar behavior has been observed for other bimetallic Pd-based catalysts with other metals, such as Sn, Ni, and Mo [10,17].

Table 2 presents the lattice parameters *a*, *b*, and *c*, volume (*V*), and the estimated crystallite sizes (*D*) for the electrocatalysts. It is important to note that PdAg electrocatalysts present intermediate values for all parameters between those of pristine Pd and Ag. These results corroborate the hypothesis of the formation of a solid solution instead of the defined crystallographic domains of Ag and Pd. The addition of metals with an atomic radius

greater than Pd (1.28 Å) to its structure, as for Ag (1.34 Å), increases the values of the lattice parameters, indicating an expansion of the crystalline lattice of Pd. Similar results are observed for other alloyed metals to Pd, such as Mo (1.29 Å), Au (1.34 Å), and Sn (1.40 Å) [23,33], whereas, the crystallite size decreases with the addition of alloyed metal atoms of larger atomic radii. This behavior is consistent with previous reports in the literature [10,16,17,23]. Yin et al. evaluated the influence of Ag concentration on the particle size and particle size distribution of Pd and observed decreasing crystallite size with increasing content of Ag [34] (see Table S1 in the Supplementary Materials), an observation in agreement with our results.

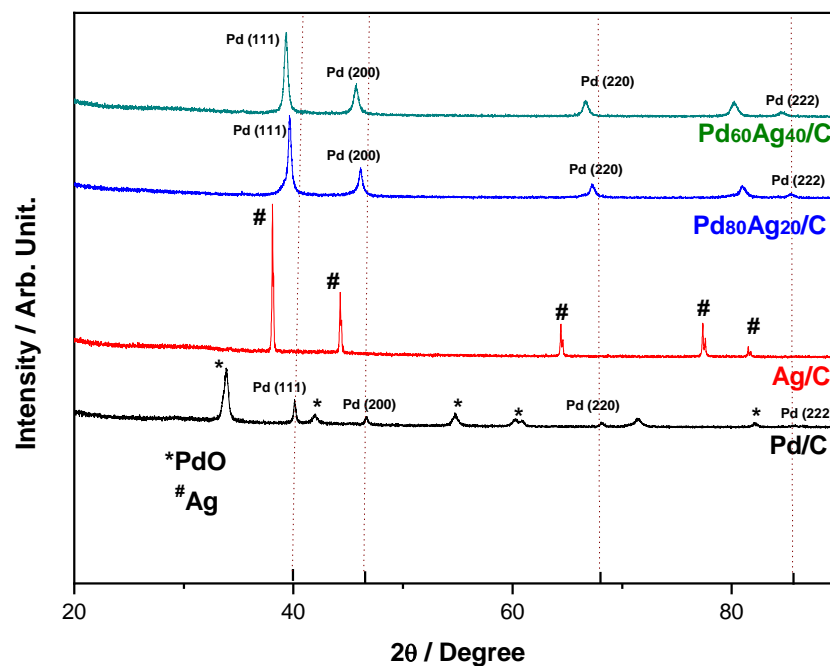


Figure 1. X-ray diffraction patterns of the electrocatalysts 40% metals-based/C; 2θ range 20–90° registering at 0.01° steps with Cu $K_{\alpha 1}$ radiation (1.54060 Å). The predicted diffraction peaks for Ag, Pd, and PdO were also included.

Table 2. Characteristic crystallographic parameter of each electrocatalyst defined from XRD analyses.

Catalyst	Phase	a = b (Å)	c (Å)	V (Å) ³	D (nm) Pd			
					(111)	(200)	(220)	(311)
Pd/C	Pd	3.89	-	58.9	40.9	29.4	21.3	16.4
	PdO	3.05	5.34	49.5	-	-	-	-
Ag/C	Ag	4.09	-	68.2	62.5	52.4	39.3	33.5
Pd ₈₀ Ag ₂₀ /C	Pd	3.91	-	59.7	31.7	24.9	18.3	15.9
Pd ₆₀ Ag ₄₀ /C	Pd	3.96	-	62.0	25.5	20.9	16.4	14.3

Lattice parameters (a, b and c), volume (V), and the estimated crystallite sizes (D) for the catalysts.

The TG/DTG analyses of Figure 2 were performed in the temperature range 273–1200 K. The loss of mass observed is associated with the oxidation of carbon that occurs in the temperature range 600–900 K, which then allows estimation of the amount of metal, based on the remaining mass of the samples [10,23,35]. The mass percentage, in combination with the EDX results, provides an accurate value of the content of Pd and Ag mass that will be used in the discussion of electrochemical properties [23]. The peaks observed in the inflections of the DTG curves identify the temperature at which the total degradation of the carbon support occurs. It is observed that the electrocatalyst Pd₆₀Ag₄₀/C presented a lower value of temperature in the inflection peak (~770 K) in relation to the other studied electrocatalysts (i.e., above 800 K). The TG curves of the Pd/C, Pd₈₀Ag₂₀/C, and Ag/C

electrocatalysts presented profiles similar to those reported by Holade et al. [35]. The estimated C and metal values are summarized in Table 3. It is important to note the good agreement between the theoretical compositions and experimental observations from the EDX analyses.

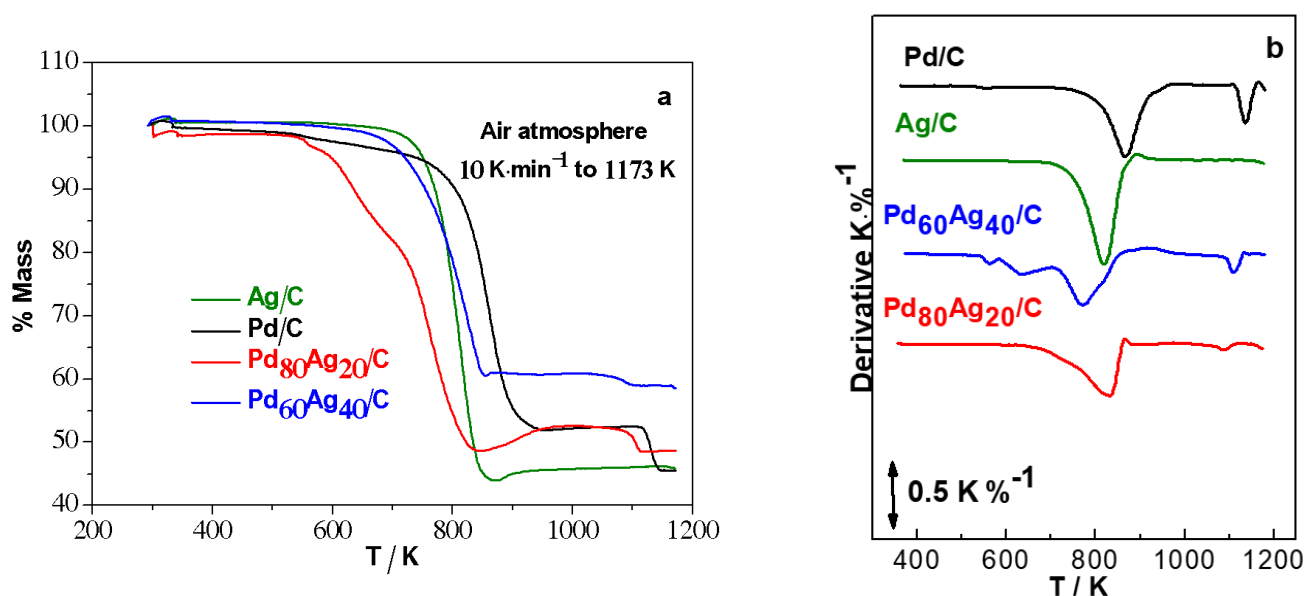


Figure 2. Thermogravimetric profiles of the electrocatalysts 40% metals-based/C—temperature range of 273–1200 K (a) TG (b) DTG.

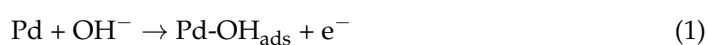
Table 3. The experimental composition was obtained by EDX, reaction yield, and thermogravimetry data for the electrocatalysts.

Nominal Composition (%)	Exp. Composition ^a (% mol)	Synthesis Yield (%)	% Exp. Metal ^b	% Exp. C ^b
Pd/C	Pd/C	97.1	45.5	54.5
Pd ₈₀ Ag ₂₀ /C	Pd ₇₉ Ag ₂₁ /C	98.6	49.0	51.0
Pd ₆₀ Ag ₄₀ /C	Pd ₅₈ Ag ₄₂ /C	96.5	58.0	42.0
Ag/C	Ag/C	97.9	46.0	54.0

^a Results estimated by EDX; ^b Estimated by TG; % metal nominal = 40% w/w; % C nominal = 60% w/w.

2.2. Benchmarking the Electrocatalytic Behavior of Bimetallic Catalysts

The electrocatalytic response was analyzed by cyclic voltammetry. Figure 3 presents the voltammetric profile of the electrocatalysts in an alkaline medium with similar anodic and cathodic current densities in the potential range between −0.8 and 0.4 V vs. SCE. This potential range was adopted since the voltammetric curve of compounds containing Pd generally presents three distinct regions during the scan (direct and/or reverse): the so-called hydrogen region, observed between −0.8 and −0.4 V vs. SCE, the oxidation region of Pd/PdO, observed in the potential range between −0.4 and 0.4 V vs. SCE (Equations (1) and (2)) [35] and the reduction of PdO, observed between −0.6 and −0.4 V vs. SCE (Equation (3)) [10,16].



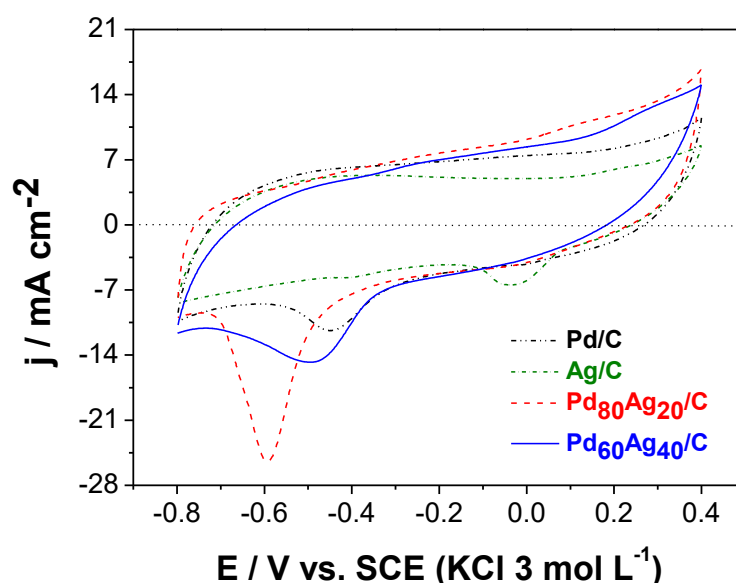


Figure 3. Cyclic voltammograms of the electrocatalysts 40% metals-based/C in N_2 -purged KOH 1.0 mol L^{-1} electrolyte at scan rate of 20 mV s^{-1} .

The pristine Pd/C clear cathodic peak (E_{cat}) observed at ca. -0.42 V vs. SCE is associated with the reduction of PdO described by reaction (3). Meanwhile, the pristine Ag/C showed a cathodic peak at approximately -0.030 V vs. SCE related to the Ag_2O reduction described by Equation (4). [35].



In contrast, the bimetallic $\text{Pd}_{80}\text{Ag}_{20}/\text{C}$ and $\text{Pd}_{60}\text{Ag}_{40}/\text{C}$ electrocatalysts showed slight differences. It can be observed in Figure 3 that E_{cat} for PdO was displaced to more negative values when compared to the Pd/C. Table 4 collects characteristic electrochemical figures of merit for easier comparison between pristine monometallic and bimetallic electrocatalysts. The observed displacement of the peak suggests an improvement of catalytic activity in the alkaline medium for both electrocatalysts. The formation of alloys and intermetallic phases have been demonstrated to enhance electrocatalytic responses. This improvement may be related to alloy formation in both bimetallic electrocatalysts, which would facilitate the electronic effect mechanism (an intrinsic mechanism) in which the presence of a second metal modifies the electronic structure of Pd, weakening its adsorption of oxygen-containing species [36–38].

Table 4. Electrochemical data obtained by cyclic voltammetry and chronoamperometry.

Electrocatalyst	m Pd (mg) ^a	E_{cat} (V) ^b	E_{onset} (V) ^c	j_{peak} (mA cm^{-2}) ^d	i_{peak} (mA mg Pd^{-1}) ^e	$j_{(-0.4 \text{ V})}$ (mA cm^{-2}) ^f	$\delta \cdot 10^{-3}$ ($\% \text{ s}^{-1}$) ^g	μ ^h	ECSA ($\text{m}^2 \text{ g}^{-1}$) ⁱ	Q (mC) ^j
Pd/C	0.501	-0.42	-0.43	17.8	23.8	12.8	-0.450	0.371	6.00	100
Ag/C	-	-0.030	-	-	-	-	-	-	-	-
$\text{Pd}_{80}\text{Ag}_{20}/\text{C}$	0.425	-0.49	-0.59	44.7	69.0	42.1	-1.36	1.10	7.62	1053
$\text{Pd}_{60}\text{Ag}_{40}/\text{C}$	0.319	-0.58	-0.61	64.8	134	53.4	-1.53	0.618	11.4	1105

^a—Estimated by EDX and TG from 1.0 mg of electrocatalyst at the working electrode; ^b—Peaks of cathodic potentials, E_{cat} (Figure 3); ^c—EOR initiation potential, E_{onset} (Figure 4); ^d—Maximum current density, j_{peak} (Figure 4); ^e—Maximum current for Pd mass (Figure S2 Supplementary Materials); ^f—Current density at -0.4 V vs. SCE , $j_{(-0.4 \text{ V})}$ (Figure 4); ^g—Poisoning rate (Equation (10)); ^h—Tolerance of catalysts (Equation (9)); ⁱ—Electrochemical surface-active area (Equation (15)); ^j—Charge involved in EOR (Equation (11)).

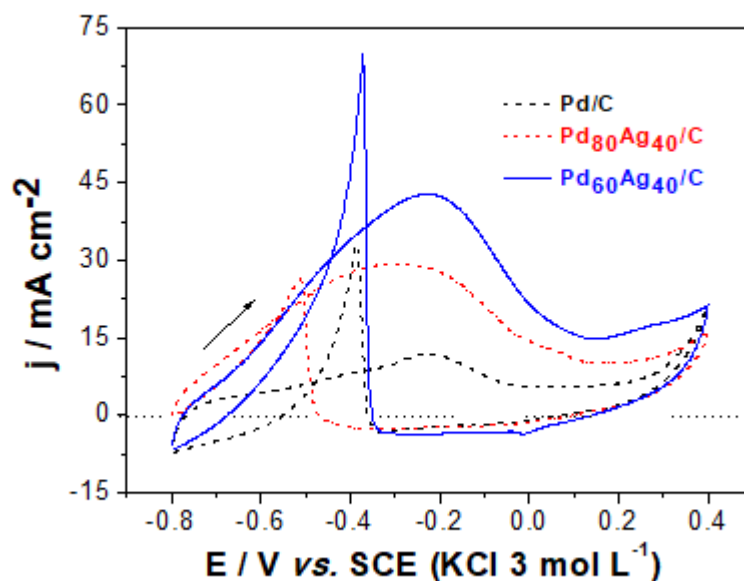
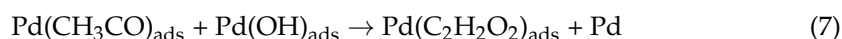


Figure 4. Cyclic voltammograms of the electrocatalysts 40% Pd-based/C in N_2 -purged KOH 1.0 mol L^{-1} /ethanol at scan rate of 20 mV s^{-1} .

The bimetallic electrocatalysts could even lead to a rate-determining step with lower activation energy, which would translate into faster electrokinetics [10,36]. The decrease in activation energy has been recently assessed through density functional theory (DFT) calculations [39]. The DFT results corroborated a strong PdAg interaction that would favor the formation of PdAg alloys with approximately equal concentrations of Pd and Ag as the energetically stable and favorable structure. The replacement of Pd by Ag leads to weaker intermetallic bonds that decrease CO adsorption and favor reactivity, according to DFT calculations [39]. Our research provides experimental support for these theoretical considerations. In Figure 3 it is possible to observe a lower E_{cat} value for the catalyst $\text{Pd}_{60}\text{Ag}_{40}/\text{C}$ in relation to $\text{Pd}_{80}\text{Ag}_{20}/\text{C}$ (Table 4), suggesting that the decrease in the amount of Pd favored the improvement of catalytic activity. The ECSA values (calculated according to Equation (15)) observed in Table 4 are related to several factors, including the crystallite size [40]. The PdAg/C electrocatalysts present higher ECSA, favoring accessibility to electrocatalytic sites on the surface, which would be in good agreement with the smaller crystallite sizes observed in the previous XRD analyses (see Table 3).

The relevant aspect of these novel bimetallic electrocatalysts is their enhanced ethanol oxidation capabilities. Figure 4 presents the electrochemical response of the electrocatalysts in alkaline solution in the presence of ethanol as fuel (Ag/C did not show electrochemical activity for EOR). Comparing the voltammograms obtained in the presence and absence of ethanol (Figure 3), the profiles of the curves have, as a differential element, the peak of ethanol oxidation as the main trait. Two peaks are observed in the voltammograms of EOR, related to ethanol oxidation. In the anodic scan, the peak observed corresponds to the oxidation of adsorbed species from the dissociative adsorption of ethanol. However, during the cathodic scan, the peak is associated with the removal of carbonaceous species that were not completely oxidized on the anodic scan [37]. According to Fornazier Filho et al. [23] and Hammed [41] the ethanol oxidation reaction on the Pd electrocatalyst results from the adsorption of ethanol on the electrocatalytic surface, where it is not completely oxidized in an alkaline medium and can be represented by Equations (5)–(8).





The values of the EOR initiation potentials (E_{onset}) collected in Table 4 indicate which are the best electrocatalysts for this process. The addition of Ag to Pd shifts the E_{onset} values towards desired, more negative, values [40]. It can be inferred from Table 4 that more negative E_{onset} values can be achieved as the amount of Ag increases. This result suggested a higher facility to initiate the ethanol oxidation [10] due to the Pd structure modification by Ag occurring in the bimetallic compositions. The values of the maximum peaks of current densities are also presented in Table 4. It can be observed that the addition of Ag promotes an increase in the values of j , demonstrating a higher catalytic activity for PdAg/C.

It was also observed that the decrease in Pd mass favored an increase in current (Table 4 and Figure S2 Supplementary Materials). Regarding the Pd₈₀Ag₂₀/C electrocatalyst, there was a decrease of approximately 15% in mass and an observed increase in current of approximately 65%. Regarding the Pd₆₀Ag₄₀/C electrocatalyst, there was a decrease in mass by approximately 36% and an observed increase in current of approximately 80%. These results confirm the improvement in the catalytic activity of the electrocatalysts with decrease in Pd mass.

The values observed in Figure 4 and Table 4 also show that the presence of PdO in the electrocatalyst structure (Figure 1) did not exert an influence or enhance the catalytic activity of the electrocatalyst, as has been reported for other oxides, such as NiO₂ [10] and RuO₂ [16,23]. The tolerance of the electrocatalysts (μ) by accumulated carbonaceous species can be described by Equation (9) [20].

$$\mu = \frac{I_f}{I_b} \quad (9)$$

where I_f is the current density peak in the anodic direction and I_b is the current density peak in the reverse direction. The higher the values of μ , the more effective is the removal of carbonaceous intermediates that poison the catalyst surface [20]. Table 4 presents the values of μ for Pd/C and PdAg/C. According to the data presented in Table 4, the value of μ for the PdAg/C is higher than Pd/C, suggesting that bimetallic electrocatalysts have greater effectiveness in removing carbonaceous intermediates that promote poisoning. This resistance to CO poisoning is of great relevance when considering the long-term application of electrocatalysts in commercial settings after technology translation.

Chronoamperometric studies can provide information to estimate the poisoning rate in ROE by calculating the slope of the straight line when the reaction stabilizes, calculate the charge involved in ROE by integrating the curve obtained in the chronoamperometry measurements, and determine which catalyst has the highest catalytic activity by comparing current density values observed for alcohol fuel cell systems [17,20,23].

As illustrated in Figure 4, the peak of ethanol oxidation in alkaline medium is characteristically wide [16,23]. The potential region between -0.6 to -0.2 V vs. SCE defines the range between the onset potential to the maximum current of the peak. Thus, -0.4 V vs. SCE defines an intermediate potential for effective benchmarking of electrocatalytic ethanol oxidation under chronoamperometric conditions. Figure 5 illustrates that Pd/C has a notably lower current response than bimetallic PdAg/C electrocatalysts, demonstrating the higher activity of PdAg/C for ethanol oxidation. It can be observed that all electrocatalysts show an accentuated decrease in current density after the first minutes of electrolysis, followed by a slight drift until the end of the analysis ($t = 7200$ s). This behavior can be ascribed to the electrocatalytic sites being blocked by smaller organic molecules resulting from ethanol oxidation (e.g., CH₃CH₂OH, CH₃CO, and CH₃COOH) [23]. The higher initial response of electrodes shows high activity given the clean surface where only ethanol is adsorbed without significant competitiveness of other molecules. However, after the initial stage, the blocking of active sites by shorter molecules (i.e., ethanol oxidation by-products) would result in a decreased rate of adsorption of new ethanol molecules. The slower adsorption rate of ethanol and ethanol availability on the electrocatalyst surface

will consequently result in a lower ratio of EOR charge transfer events, with consequent decrease in the current response. Further analysis of Figure 5 shows that stabilization occurs in approximately 250, 700, and 850 s for Pd/C, Pd₈₀Ag₂₀/C, and Pd₆₀Ag₄₀/C, respectively. From these stabilization times, the variation in the surface poisoning rate (δ) can be estimated from Equation (10) in units of % change s⁻¹ [16,23]:

$$\delta = \frac{100}{j} \frac{\Delta j}{\Delta t} \quad (10)$$

where $\Delta j/\Delta t$ is the rate of change in the slope of the linear portion of the current density decline, and j is the current density at -0.4 V vs. SCE (Figure 5). The δ values collected in Table 4 demonstrate that the addition of Ag shifts the poisoning rate values to more negative values, suggesting that there is an Ag contribution to decreasing the poisoning of PdAg/C in relation to Pd/C. The synergistic role of Ag in the allowed structure of bimetallic PdAg/C electrocatalysts can be explained by the modification of the electronic structure of Pd, decreasing both the poisoning of the active sites and the activation energy of EOR [29,30,40]. These results are consistent with the CV results, where PdAg showed higher catalytic activity (Figure 4 and Table 4).

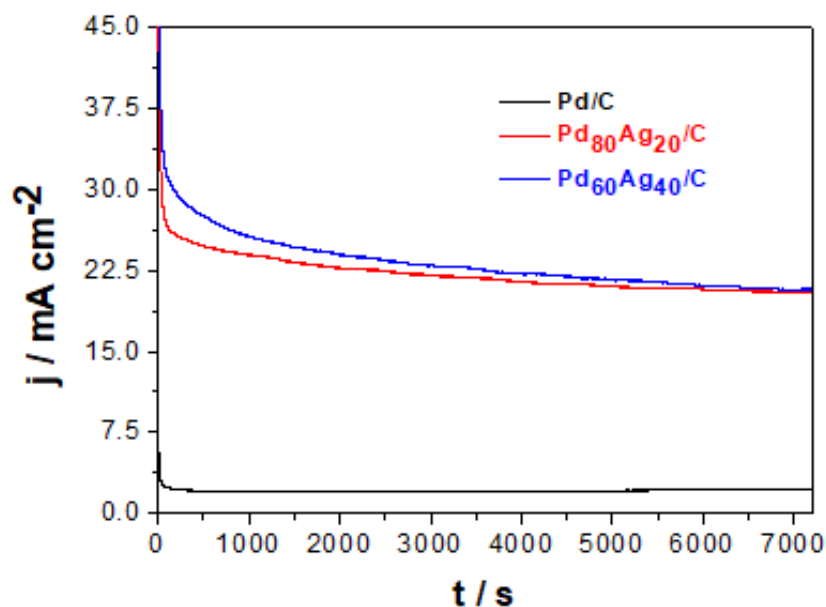


Figure 5. Chronoamperometry curves of the electrocatalysts 40% Pd-based/C in N₂-purged KOH 1.0 mol L⁻¹/ethanol electrolyte at -0.4 V vs. SCE.

The charge Q involved in EOR can be calculated by integrating the area under the curve on the chronoamperometry experiment from Equation (11):

$$Q = \int_0^{7200} j dt \quad (11)$$

The analysis of Q corroborates the enhanced performance of bimetallic catalysts that present an over 10-fold higher charge circulation associated with ethanol oxidation through EOR.

2.3. Understanding Poisoning Resistance through CO Stripping

Carbon monoxide (CO) is an intermediate of the incomplete oxidation on the EOR in fuel cells at low temperatures, being responsible for the poisoning of the electrocatalyst surface. In this context, the study of CO tolerance on Pd/C, Pd₈₀Ag₂₀/C, and Pd₆₀Ag₄₀/C was performed to evaluate the behavior of these electrocatalysts when contaminated with

CO. Evaluation of CO tolerance is conventionally evaluated in terms of the initial potential of ethanol oxidation to CO-species. The more negative the initial potential of oxidation of CO adsorbed on the electrocatalyst, the better is its performance for EOR [42].

Figure 6 presents the CO stripping curves of Pd/C, Pd₈₀Ag₂₀/C, and Pd₆₀Ag₄₀/C electrocatalysts. The peak observed in the first cycle is related to CO adsorption on the electrocatalyst surface. The onset potential of CO adsorption is displaced to a more negative potential when increasing the silver content in the electrocatalysts. The onset potentials of CO adsorption at -0.286 , -0.419 , and -0.484 V are shown for Pd/C, Pd₈₀Ag₂₀/C, and Pd₆₀Ag₄₀/C, respectively. The lower value of the onset potential of Pd₆₀Ag₄₀/C indicates that this electrocatalyst had a greater ability to remove the CO intermediate from the Pd active sites, facilitating the EOR. These results agree with the chronoamperometric results (Figure 5 and Table 4), in which Pd₆₀Ag₄₀/C was found to be less susceptible to CO poisoning. Overall, the benefits of eased CO removal from the surface and lower CO poisoning align to enhance the electrocatalytic performance and the sustained response over time. The experimental results suggest that Pd₆₀Ag₄₀/C is more effective for EOR given the alloyed Pd-Ag phases.

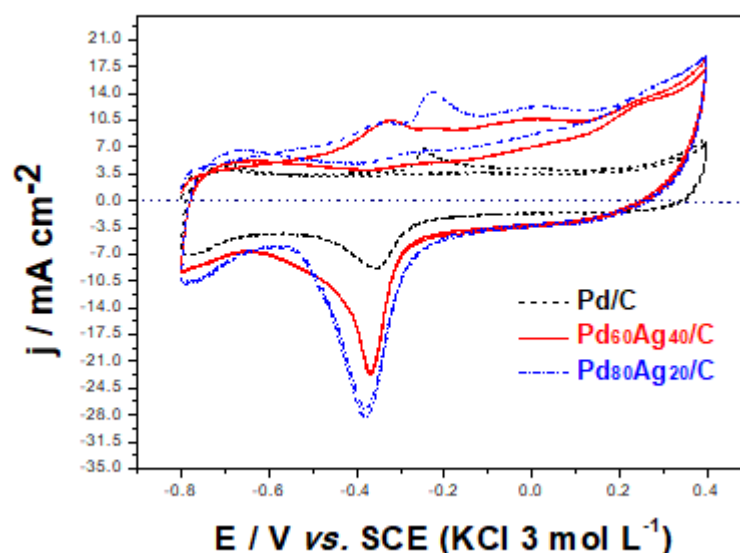


Figure 6. CO-stripping of the electrocatalysts 40% Pd-based/C in KOH 1.0 mol L⁻¹ at scan rate of 20 mV s⁻¹.

The results observed in this study suggest that the electrocatalyst Pd₆₀Ag₄₀/C presented a better catalytic performance for EOR. As proposed by Mostashari et al. [40], the improvement in the catalytic performance of PdAg/C electrocatalysts can be explained by the following factors: better dispersion of the particles in the support material, formation of PdAg solid solution, and increased ECSA. From the results presented by XRD (Figure 1), the diffraction angles of the bimetallic electrocatalysts are shifted to lower values. This shift demonstrates the alteration of the crystalline structure and hints at the formation of alloys (solid solutions). Solid solutions of metals at the interface can favor the adsorption of OH⁻ on the Pd surface and facilitate the removal of CO-type intermediate species, releasing the active sites on the surface of the electrocatalyst surface [40]. It is also reported that the excellent catalytic activity is related to the alloy composition and electronic structure modulation by d-band electronic effects, with strong synergistic effects observed for the PdAg binary alloy. It can be concluded that the addition of Ag to Pd favors the intrinsic mechanism [43–45], a catalysis mechanism that results in a modification of the electronic properties of Pd by a second or third metal. In this mechanism, the 5d bands are emptied or filled, and this effect causes a decrease in the binding strength of CO on the catalyst surface, weakening its adsorption of oxygen-containing species. This is a theoretical result predicted by DFT calculations [39] where the favoring of an energetically stable and favorable

structure was observed for PdAg alloys with approximately equal concentrations of Pd and Ag. It was also reported that higher ECSA values expose the electrocatalyst surface to numerous active sites and EOR is facilitated [43]. Therefore, the better catalytic performance of Pd₆₀Ag₄₀/C may be related to several factors: the smaller crystallite size [10] (Table 2), solid solution formation, intrinsic mechanism, and higher ECSA (Table 4).

2.4. Feasibility and Economy

The results presented and discussed in Table 4, Figures 3–5 showed that, as predicted by theoretical calculations [39], by decreasing the amount of Pd and increasing Ag, it was possible to obtain better electrochemical results for EOR. With a view to understanding the Pd salt economy, Table 5 presents an estimate of the expected economics for the electrocatalysts studied in this study, in which \$ is the average value of the amount of Pd in the respective catalyst, assuming a value of USD 150.00/g of Pd salt (Pd(NO₃)₂·2H₂O) [45], and Δ\$ is the percentage of the cost of PdAg/C catalysts in relation to Pd/C.

Table 5. Estimated savings for PdAg/C electrocatalysts compared to Pd/C, considering a value of USD 150.00/g of Pd salt *.

Electrocatalyst	m Pd (mg)	\$ ^a (US\$)	Δ\$ ^b (%)
Pd/C	0.501	0.0752	-
Pd ₈₀ Ag ₂₀ /C	0.425	0.0638	15.2
Pd ₆₀ Ag ₄₀ /C	0.319	0.0479	36.6

^a Average value in USD in relation to the amount of Pd in the electrocatalyst; ^b Percentage of cost reduction in relation to Pd/C; * Pd(NO₃)₂·2H₂O.

Relating the values observed in Tables 4 and 5, Figures 3–5, it can be suggested that the catalyst Pd₆₀Ag₄₀/C presented the most promising results. This implies that the synthesis method studied in this study has been shown to be feasible for the synthesis of PdAg catalysts combining Pd salt, which has a high market value, with Ag salt, a cheaper material. Therefore, the technique of thermal decomposition of polymeric precursors is confirmed to be efficient for the reduction of the amount of palladium salt in the synthesis, both economically and in terms of electrochemical activity. For comparison purposes, Table 6 presents a brief summary of results observed in the literature for PdAg catalysts and the Pd₆₀Ag₄₀/C evaluated in this study.

Table 6. Comparison between some PdAg electrocatalysts presented in the literature with Pd₆₀Ag₄₀/C evaluated in this study.

Used Technique	Remarks on the Amount of Pd or Ag	References
Thermal decomposition of polymeric precursors	Best catalytic activity for Pd ₆₀ Ag ₄₀	This study
Electroless method	Best catalytic activity for Pd ₇₉ Ag ₂₁	[27]
Impregnation-reduction	Best catalytic activity for 25–33% of Ag	[29]
Synthesis using ethanolic NaOH	Best catalytic activity for Pd ₃ Ag ₁	[40]
Hydrothermal	Best catalytic activity for Pd ₄ Ag ₁	[46]
CL bromide	Best catalytic activity for Pd ₂ Ag ₁	[47]
Reduction for NaBH ₄	Best catalytic activity for Pd ₆₇ Ag ₃₃	[48]
Synthesis using DODAC as a surfactant template and AA as a reductant	Best catalytic activity for Pd ₂ Ag ₁	[49]

Observing the results presented in Tables 5 and 6, it is possible to conclude that Pd₆₀Ag₄₀/C produced by the technique of thermal decomposition of polymeric precursors has been shown to be a viable alternative for anodes in fuel cells in EOR [27,29,40,46–49], because it requires lower amounts of Pd with good catalytic activities and consequent economy in the cost of the Pd salt.

3. Materials and Methods

3.1. Chemicals and Materials

Precursor salts Pd(NO₃)₂·2H₂O 99%, AgNO₃ 99% were purchased from Sigma-Aldrich (Budimpest, Hungary). Nafion™ 117 solution and anhydrous citric acid (C₆H₈O₇) (CA) 99.5% were acquired from Sigma-Aldrich (Budimpest, Hungary). The carbon Vulcan XC72 used as catalyst support was provided by Carbot (Billerica, MA, USA). Other chemicals used in this study were provided by different suppliers: ethanol 99.9% (Vetec—São Paulo, Brazil), ethylene glycol (EG) 99.8% (Dinâmica, Cotia, Brazil), alumina suspension n° 3–0.3 μm (Skill-Tec, São Paulo, Brazil), KOH (Proquímios—Duque de Caxias, Brazil), HNO₃ 65% (Neon, São Paulo, Brazil), N₂ 5.0–99.9% purity (White Martins—Serra, Brazil), and CO 4.0–99.9% purity (White Martins—Serra, Brazil). Ultrapure water purified in the equipment Sartorius mini, Arium™, model MA-UVT (São Bernado do Campo, Brazil) with a resistivity of 18.0 MΩ cm at 22 °C was used to prepare all the solutions for the synthesis and electrochemical tests.

3.2. Electrocatalysts Preparation

Carbon Vulcan XC72 was selected as the substrate for the metallic catalysts given its extensive use in fuel cells. The material selection criteria for carbon Vulcan XC72 was based on its excellent properties as a substrate with outstanding conductivity at relatively low charge levels and the ease of dispersion of the metals on its surface. It has been reported that its treatment with HNO₃ improved the catalytic activity of electrocatalysts, suggesting that the treated carbon may assist in the transport of ions in the reaction phase, improving the continuity of the oxireduction reactions [10,23].

Pd/C, Ag/C, and PdAg/C electrocatalysts were synthesized by thermal decomposition of a polymeric precursor coating. Briefly, carbon Vulcan XC72 (C_{vulcan}) used as support was treated with 100 mL of a 2.0 molL⁻¹ HNO₃ solution and kept in an ultrasonic bath for 30 min. Afterwards, the mixture was stirred at reflux at 80 °C for 24 h and filtered under vacuum [23]. Then, specific precursor mixtures were prepared to attain a theoretical molar ratio in the final catalyst corresponding to Pd₁₀₀/C (termed Pd/C), Ag₁₀₀/C (termed Ag/C), Pd₈₀Ag₂₀/C, and Pd₆₀Ag₄₀/C. Note that calculations were conducted considering that the C_{vulcan} will correspond to 60% of the final mass [23,50], and the remaining 40% will correspond to the metals (Pd and Ag). The required mass of each metal was calculated from their respective molar fractions using Equation (12):

$$m_i = x_i M_i \left(\frac{m_t}{\sum M_i} \right) \quad (12)$$

where m_i is the mass of species i ($i = \text{Ag}$ or Pd), M_i is the molar mass, x_i is the molar fraction, and m_t is the total metal mass. To prepare the precursor polymeric solution, Pd(NO₃)₂·2H₂O and AgNO₃ were mixed in a solution of citric acid and ethylene glycol at a 1:4:16 molar ratio and then added to C_{vulcan} [23]. The formed suspension was stirred at approximately 353–363 K for 2 h. After this time, the suspension temperature was raised to 403 K and later left to dry. Subsequently, the samples were placed in an oven and annealed at 573 K until constant mass was reached (evaluating mass loss every 5 min). Detailed information is provided in the Supplementary Materials.

3.3. Material Characterization

The obtained electrocatalysts were characterized. XRD diffractograms were recorded in a Bruker D8 Advance diffractometer within a 2θ range 10–90° registering at 0.01° steps with a Cu K_{α1} radiation (1.54060 Å) source. The diffractograms were evaluated using the program “Evolution” (EVA) (Bruker™) obtaining characteristic crystallographic planes and lattice parameters. The crystallite size was estimated using the Scherrer equation [23,24,51]. Scanning electron microscopy (SEM) images were acquired on a Jeol JSM 6610L microscope coupled with energy dispersive X-Ray analysis (EDX). Samples were prepared before

SEM/EDX analyses by adding the electrocatalyst samples on a carbon strip attached to an aluminum holder and covered with gold using a Denton Vacuum Desk V metallizer. Thermal analysis was processed on a Shimadzu TGA50-H thermal analyzer under a synthetic air atmosphere at a heating rate of $283 \text{ K}\cdot\text{min}^{-1}$ from 298 to 1173 K.

3.4. Electrochemical Characterization

Cyclic voltammetry (CV) and chronoamperometry (CA) were performed with a glassy carbon working electrode (area 0.066 cm^2) with catalyst ink, a graphite counter electrode (area 12.05 cm^2), and a saturated calomel electrode (SCE) (Analyzer, model 3A41) as a reference electrode. The working electrode was previously polished with an alumina suspension (n° 3–0.3 μm Skill-Tec). Electrocatalysts were deposited by drop-casting on the polished working electrode surface and dried at 60°C . Catalytic inks were composed of 1.0 mg of electrocatalyst, 95 μL ethanol, and 5 μL of NafionTM 117 solution, all homogenized for 30 min in an ultrasonic bath.

CV measurements were performed using a PAR-Ametek VersaStat 4TM potentiostat/galvanostat in the potential range from -0.8 to 0.4 V vs. SCE, 2 cycles with a scan rate of $20 \text{ mV}\cdot\text{s}^{-1}$ for KOH 1.0 mol L^{-1} and a solution composed of 5.83 mL ethanol and 100 mL KOH 1.0 mol L^{-1} . CA was performed by applying a fixed potential at -0.4 V vs. SCE for 2 h to a solution composed of 5.83 mL ethanol and 100 mL KOH 1.0 mol L^{-1} . The electrolytes were purged with N_2 for 10 min before each CV measurement.

For the CO-stripping voltammetry, the electrochemical cell was assembled using SCE as reference electrode and KOH $1.0 \text{ mol}\cdot\text{L}^{-1}$ solution as the electrolyte, using the Vertex potentiostat/galvanostat controlled through Ivium softwareTM. A fixed potential at -0.4 V was applied for 15 min with the passage of CO. To obtain the CV curves, they were performed in the potential range between -0.8 and 0.4 V vs. SCE with a scan rate of 20 mV s^{-1} . The excess of CO from the electrolyte was removed using N_2 .

The electrochemical active surface area (ECSA) was calculated using the PdO reduction region in the CV-curves because it cannot be obtained in the hydrogen adsorption/desorption region [52]. The calculation of the charge (q) used for PdO reduction was performed using Equation (13).

$$q = \frac{A}{v} \quad (13)$$

where A is the area of PdO reduction peak and v is the scan rate used in the CV. The surface area (SA) was calculated using Equation (14).

$$SA = \frac{q}{q_{Pd}} \quad (14)$$

where q_{Pd} has a constant reported value of 0.405 mC cm^{-2} [10]. Then, the ECSA was calculated using Equation (15), where m is the mass of Pd deposited on the working electrode.

$$ECSA = \frac{SA}{m} \quad (15)$$

4. Conclusions

This paper reports a facile stoichiometric control of the synthesis of PdAg/C electrocatalysts based on the thermal decomposition of polymeric precursors. Synthesized electrocatalysts presented an excellent electrocatalytic response as an anode in fuel cells for ethanol oxidation. The material characterization demonstrated that the synthesis method enabled the formation of bimetallic PdAg electrocatalysts with alloyed phases. The formation of a solid solution of PdAg resulted in a beneficial arrangement of bimetallic electrocatalytic sites that minimized CO poisoning and enhanced their recovery through stripping. The experimental results demonstrated the higher electrocatalytic activity of PdAg/C electrocatalysts when benchmarked against pristine Pd.

Bimetallic electrocatalysts of PdAg/C demonstrated a lower poisoning rate and sustained stability for a longer time. Furthermore, bimetallic catalysts enabled faster surface regeneration driven by CO complete oxidation to CO₂. The Pd₆₀Ag₄₀/C composition was identified as the most competitive stoichiometric composition in terms of electrocatalytic response. Pd₆₀Ag₄₀/C showed an increase of ~3.3% on ΔE_{onset} and ~31.1% on Δj_{peak} , with respect to pristine Pd/C. Therefore, the method of thermal decomposition of polymeric precursors has been shown to be an efficient method of synthesis that provides accurate control over bimetallic catalyst composition. The results demonstrate that, through this alternative method, it is possible to minimize the content of Pd while maximizing the electrocatalytic response.

Supplementary Materials: The following are available online at <https://www.mdpi.com/article/10.3390/catal12010096/s1>: Table S1: Amount of the reagents used for the synthesis of each electrocatalyst; Table S2: Atomic compositions of electrocatalysts obtained by EDX; Figure S1: SEM micrographs of electrocatalysts; Figure S2: Cyclic voltammograms of the electrocatalysts (mA mgPd⁻¹); Figure S3: Chronoamperometry curves of the electrocatalysts (mA mgPd⁻¹).

Author Contributions: Conceptualization, Y.F.F. and J.R.; methodology, Y.F.F., A.C.C.d.C., R.V.R., J.R.C.S., R.P., P.P.L., S.G.-S. and J.R.; funding acquisition, Y.F.F., P.P.L. and J.R.; investigation, Y.F.F., A.C.C.d.C., R.V.R., J.R.C.S., R.P., P.P.L., S.G.-S. and J.R.; validation, Y.F.F., A.C.C.d.C., R.V.R., J.R.C.S., R.P., P.P.L., S.G.-S. and J.R.; formal analysis, Y.F.F., A.C.C.d.C. and R.V.R.; data curation, Y.F.F., P.P.L. and J.R.; investigation, Y.F.F., A.C.C.d.C., R.V.R., J.R.C.S., R.P., P.P.L., S.G.-S. and J.R.; resources, Y.F.F., P.P.L. and J.R.; visualization, Y.F.F., A.C.C.d.C., R.V.R., J.R.C.S., R.P., P.P.L., S.G.-S. and J.R.; writing—original draft, Y.F.F. and R.V.R.; writing—review and editing, J.R.C.S., R.P., P.P.L., S.G.-S. and J.R.; supervision, J.R.; project administration, J.R. All authors have read and agreed to the published version of the manuscript.

Funding: This research was enabled by a grant from Brazilian agencies FAPES (Fundação de Amparo à Pesquisa e Inovação do Espírito Santo (FAPES n° 515/2016)—EDITAL FAPES/CAPES n° 08/2017—PROCAP—DOUTORADO), CAPES (Coordenação de Aperfeiçoamento de Pessoal de Nível Superior) and CNPq (Conselho Nacional de Desenvolvimento Científico e Tecnológico).

Data Availability Statement: Data is contained within the article or Supplementary Materials.

Acknowledgments: The authors thank the Brazilian agencies, FAPES (Fundação de Amparo à Pesquisa e Inovação do Espírito Santo (FAPES n° 515/2016)—EDITAL FAPES/CAPES n° 08/2017—PROCAP—DOUTORADO), CAPES (Coordenação de Aperfeiçoamento de Pessoal de Nível Superior) and CNPq (Conselho Nacional de Desenvolvimento Científico e Tecnológico) for financial support. We also thank the laboratories responsible for the characterization of the developed materials: LPT/LMC—Physics Department (UFES) and Laboratory of Thermal Analysis, Ivo Giolito, (LATIG—USP) for thermal analysis; Labpetro—Chemistry Department (UFES) for XRD measurements (Technical cooperation agreement 0050.0022844.06.4 and CT-Infra 01/2007-FINEP 0202/08); and Luccar (Morphology Department—CSS/UFES) for SEM/EDX.

Conflicts of Interest: The authors declare no conflict of interest.

References

1. Xu, J.B.; Zhao, T.S.; Shens, Y.; Li, Y.S. Stabilization of the palladium electrocatalyst with alloyed gold for ethanol oxidation. *Int. J. Hydrogen Energy* **2010**, *35*, 6490–6500. [[CrossRef](#)]
2. Soloveichik, G.L. Liquid fuel cells. *Beilstein J. Nanotechnol.* **2014**, *5*, 1399–1418. [[CrossRef](#)] [[PubMed](#)]
3. Antolini, E. Structural parameters of supported fuel cell catalysts: The effect of particle size, inter-particle distance and metal loading on catalytic activity and fuel cell performance. *Appl. Catal. B* **2016**, *181*, 298–313. [[CrossRef](#)]
4. Torrero, J.; Montiel, M.; Peña, M.A.; Obón, P.; Rojas, S. Insights on the electrooxidation of ethanol with Pd-based catalysts in alkaline electrolyte. *Int. J. Hydrogen Energy*. *Int. J. Hydrogen Energy* **2019**, *44*, 31995–32002. [[CrossRef](#)]
5. Santos, D.M.; Paganoto, G.T.; Queiroz, M.A.R.; Guimarães, M.C.C.; Ribeiro, J. Influence of Support material of PtSnNiGa/C Electrocatalysts for Ethanol Oxidation. *Orbital Electron. J. Chem.* **2017**, *9*, 140–150. [[CrossRef](#)]
6. Monyoncho, E.A.; Woo, T.K.; Baranova, E.A. Ethanol electrooxidation reaction in alkaline media for direct ethanol fuel cells. *Electrochemistry* **2018**, *15*, 1–57. [[CrossRef](#)]
7. Dutta, A.; Mahapatra, S.S.; Datta, J.S.S.S. High performance PtPdAu nano-catalyst for ethanol oxidation in alkaline media for fuel cell applications. *Int. J. Hydrogen Energy* **2011**, *36*, 14898–14906. [[CrossRef](#)]

8. Cai, J.; Huang, Y.; Guo, Y. Bi-modified Pd/C catalyst via irreversible adsorption and its catalytic activity for ethanol oxidation in alkaline medium. *Electrochim. Acta* **2013**, *99*, 22–29. [[CrossRef](#)]
9. Du, W.; Mackenzie, K.E.; Milano, D.F.; Deskins, N.A.; Su, D.; Teng, X. Palladium-Tin Alloyed Catalysts for the Ethanol Oxidation Reaction in an Alkaline Medium. *ACS Catal.* **2012**, *2*, 287–297. [[CrossRef](#)]
10. Moraes, L.P.R.; Matos, B.R.; Radtak, C.; Santiago, E.I.; Fonseca, F.C.; Amico, S.C.; Malfatti, C.F. Synthesis and performance of palladium-based electrocatalysts in alkaline direct ethanol fuel cell. *Int. J. Hydrogen Energy* **2016**, *41*, 6457–6468. [[CrossRef](#)]
11. Sheikh, S.Y.; Silva, E.L.; Moraes, L.; Antonini, L.M.; Abellah, M.Y.; Malfatti, C.F. Pd-based Catalysts for Ethanol Oxidation in Alkaline Electrolyte. *Am. J. Min. Metall.* **2014**, *2*, 64–69. [[CrossRef](#)]
12. Zhao, X.; Zhang, J.; Wang, L.; Liu, Z.; Chem, J. Pd_xCu_{100-x} networks: An active and durable electrocatalyst for ethanol oxidation in alkaline medium. *J. Mat. Chem. A* **2014**, *2*, 20933–20988. [[CrossRef](#)]
13. Souza, F.M.; Böhnsted, P.; Pinheiro, V.S.; Oliveira, L.A.; Batista, B.L.; Parreira, L.S.; Antunes, R.A.; Santos, M.C. Niobium increasing the electrocatalytic activity of palladium for alkaline direct ethanol fuel cell. *J. Electroanal. Chem.* **2020**, *858*, 113824. [[CrossRef](#)]
14. Chen, Y.; Zhuang, L.; Lu, J. Non-Pt Anode Catalysts for Alkaline Direct Alcohol Fuel Cells. *Chin. J. Catal.* **2007**, *28*, 870–874. [[CrossRef](#)]
15. Ma, L.; He, H.; Hsu, A.; Chen, R. PdRu/C catalysts for ethanol oxidation in anion-exchange membrane direct ethanol fuel cells. *J. Power Sour.* **2013**, *241*, 696–702. [[CrossRef](#)]
16. Carrión-Satorre, S.; Mantiel, M.; Escudero-Cid, R.; Fierro, J.L.G.; Fatás, E.; Ocan, P. Performance of carbon-supported palladium and palladium ruthenium catalysts for alkaline membrane direct ethanol fuel cells. *Int. J. Hydrogen Energy* **2016**, *41*, 8954–8962. [[CrossRef](#)]
17. Fariba, F.; Afzali, D. Bimetallic Pd–Mo nanoalloys supported on Vulcan XC-72R carbon as anode catalysts for direct alcohol fuel cell. *Int. J. Hydrogen Energy* **2017**, *42*, 3215–3221. [[CrossRef](#)]
18. Goel, J.; Basu, S. Effect of support materials on the performance of direct ethanol fuel cell anode catalyst. *Int. J. Hydrogen Energy* **2014**, *39*, 15956–15966. [[CrossRef](#)]
19. Wen, C.; Wei, Y.; Tang, D.; Sa, B.; Zhang, T.; Changxin Chen, C. Improving the electrocatalytic properties of Pd-based catalyst for direct alcohol fuel cells: Effect of solid solution. *Sci. Rep.* **2017**, *7*, 4907. [[CrossRef](#)]
20. Peng, C.; Hu, Y.; Liu, M.; Zheng, Y. High electrocatalytic activity for ethanol oxidation in alkaline media. *J. Power Sour.* **2015**, *278*, 69–75. [[CrossRef](#)]
21. Zhu, C.; Wen, D.; Oschatz, M.; Halzchuh, M.; Liu, W.; Herrmann, A.K.; Simon, F.; Kaskel, S.; Eychmüller, A. Kinetically Controlled Synthesis of PdNi Bimetallic Porous Nanostructures with Enhanced Electrocatalytic Activity. *Small Sci.* **2015**, *11*, 1430–1434. [[CrossRef](#)] [[PubMed](#)]
22. Wang, T.; Chutia, A.; Brett, D.; Shearing, P.; He, G.; Chai, G.; Parkin, I. Palladium alloys used as electrocatalysts for the oxygen reduction reaction. *Energy Environ. Sci.* **2015**, *14*, 2639–2669. [[CrossRef](#)]
23. Fornazier Filho, Y.; da Cruz, A.C.C.; Pedicini, R.; Salgado, J.R.C.; Luz, P.P.; Ribeiro, J. Development of palladium catalysts modified by ruthenium and molybdenum as anode in direct ethanol fuel cell. *Mater. Renew. Sustain. Energy* **2021**, *10*, 5. [[CrossRef](#)]
24. Ramanathan, M.; Li, B.; Greeley, J.; Prakash, J. Microstructure-ORR Activity Relationships in Pd₃M (M = Cu, Ni, Fe) Electrocatalysts Synthesized at Various Temperatures. *ECS Trans.* **2010**, *33*, 181. [[CrossRef](#)]
25. Kibler, A.; El-Aziz, A.M.; Hoyer, R.; Kolb, D.M. Tuning Reaction Rates by Lateral Strain in a Palladium Monolayer. *Angew. Chem.* **2005**, *44*, 2080–2084. [[CrossRef](#)] [[PubMed](#)]
26. Nguyen, A.T.N.; Shim, J.H. Facile one-step synthesis of Ir-Pd bimetallic alloy networks as efficient bifunctional catalysts for oxygen reduction and oxygen evolution reactions. *J. Electroanal. Chem.* **2018**, *827*, 120–127. [[CrossRef](#)]
27. Oliveira, M.; Rego, R.; Fernandes, L.; Tavares, P. Evaluation of the catalytic activity of Pd-Ag alloys on ethanol oxidation and oxygen reduction reactions in alkaline medium. *J. Power Sour.* **2011**, *196*, 6092–6098. [[CrossRef](#)]
28. Godínez-García, A.; Pérez-Robles, J.F.; Martínez-Tejada, H.V.; Solorza-Feria, O. Characterization and electrocatalytic properties of sonochemical synthesized PdAg nanoparticles. *Mat. Chem. Phys.* **2012**, *134*, 1013–1019. [[CrossRef](#)]
29. Carrera-Cerritos, R.; Salazar-Hernandez, C.; Galindo-Esquivel, I.R.R.; Fuentes-Ramirez, R. Effect of the Reduction Temperature of PdAg Nanoparticles during the Polyol Process in the Ethanol Electrooxidation Reaction. *J. Nanomater.* **2018**, *2018*, 1–9. [[CrossRef](#)]
30. Nguyen, M.T.X.; Huynh, H.K.P.; Dang, H.Q.; Nguyen, H.T.; Lee, C.T.; Pham, Y.N.; Luu, T.H.; Nguyen, S.T. Microwave Heated Synthesis of PdAg Core-Shell Nanowires for Electrochemical Oxidation of Ethanol in Alkaline Medium. *Chem. Eng. Trans.* **2020**, *78*, 169–174. [[CrossRef](#)]
31. Li, G.; Jiang, L.; Jiang, Q.; Wang, S.; Sun, G. Preparation and characterization of Pd_xAg_y/C electrocatalysts for ethanol electrooxidation reaction in alkaline media. *Electrochim. Acta* **2011**, *56*, 7703–7711. [[CrossRef](#)]
32. Feng, Y.; Zhang, K.; Yan, B.; Li, S.; Du, Y. Hydrothermal Method Using DMF as a Reducing Agent for the Fabrication of PdAg Nanochain Catalysts towards Ethanol Electrooxidation. *Catalysts* **2016**, *6*, 103. [[CrossRef](#)]
33. He, Q.; Chen, W.; Mukerjee, S.; Chen, S.; Lauef, F. Carbon-supported PdM (M = Au and Sn) nanocatalysts for the electrooxidation of ethanol in high pH media. *J. Power Sour.* **2009**, *187*, 298–304. [[CrossRef](#)]
34. Yin, Z.; Zhang, Y.; Chen, K.; Li, J.; Li, W.; Tang, P.; Zhao, H.; Zhu, Q.; Bao, X.; Ma, D. Monodispersed bimetallic PdAg nanoparticles with twinned structures: Formation and enhancement for the methanol oxidation. *Sci. Rep.* **2014**, *4*, 4288. [[CrossRef](#)]
35. Holade, Y.; Morais, C.; Arrii-Clacens, S.; Servat, K.; Napporn, T.W.; Kokoh, K.B. New Preparation of PdNi/C and PdAg/C Nanocatalysts for Glycerol Electrooxidation in Alkaline Medium. *Electrocatalysis* **2013**, *4*, 167–178. [[CrossRef](#)]

36. Gomez, J.C.C.; Moliner, R.; Lázaro, M.J. Palladium-Based Catalysts as Electrodes for Direct Methanol Fuel Cells: A Last Ten Years Review. *Catalysts* **2016**, *6*, 130. [[CrossRef](#)]
37. Iwasita, T. Electrocatalysis of methanol oxidation. *Electrochim. Acta* **2002**, *47*, 3663–3674. [[CrossRef](#)]
38. Christensen, P.A.; Hamnett, A.; Troughton, G.L. The role of morphology in the methanol electro-oxidation reaction. *J. Electroanal. Chem.* **1993**, *362*, 207–218. [[CrossRef](#)]
39. Mancera, L.A.; Behm, R.J.; Grob, A. Structure and local reactivity of PdAg/Pd (111) surface alloys. *Phys. Chem. Chem. Phys.* **2013**, *15*, 1497–1508. [[CrossRef](#)]
40. Mostashari, S.M.; Dehkharghani, R.A.; Afshar-Taromi, F.; Farsadrooh, M. A straightforward one-pot synthesis of Pd–Ag supported on activated carbon as a robust catalyst toward ethanol electrooxidation. *Int. J. Hydrogen Energy* **2021**, *46*, 9406–9416. [[CrossRef](#)]
41. Hammed, R.M.A. Enhanced ethanol electro-oxidation reaction on carbon supported Pd-metal oxide electrocatalysts. *J. Colloid. Interface Sci.* **2017**, *505*, 230–240. [[CrossRef](#)]
42. Chatterjee, S.; Griego, C.D.; Hart, J.; Li, Y.; Taheri, M.; Keith, J.; Snyder, J. Free Standing Nanoporous Palladium Alloys as CO Poisoning Tolerant Electrocatalysts for the Electrochemical Reduction of CO₂ to Formate. *ACS Catal.* **2019**, *9*, 5290–5301. [[CrossRef](#)]
43. Lin, R.; Ma, X.; Cheong, W.C.; Zhang, C.; Zhu, W.; Pei, J.; Wang, B.; Liang, S.; Liu, Y.; Zhuang, Z.; et al. PdAg bimetallic electrocatalyst for highly selective reduction of CO₂ with low COOH* formation energy and facile CO desorption. *Nano Res.* **2019**, *12*, 2866–2871. [[CrossRef](#)]
44. Navlani-García, M.; Salinas-Torres, D.; Cazorla-Amorós, D. Hydrogen Production from Formic Acid Attained by Bimetallic Heterogeneous PdAg Catalytic Systems. *Energy* **2019**, *12*, 4027. [[CrossRef](#)]
45. Merck Brazil. Available online: https://www.merckmillipore.com/Web-BR-Site/pt_BR/-/BRL/ViewUserAccount (accessed on 30 September 2021).
46. Gao, F.; Yin, Y.; Cao, Z.; Li, H.; Guo, P. Chemical Design and Environmental/Energetic Applications of Self-Assembled Nanocomposites and Nanostructures. *J. Chem.* **2020**, *2020*, 1917380. [[CrossRef](#)]
47. Yang, M.; Lao, X.; Sun, J.; Ma, N.; Wang, S.; Ye, W.; Guo, P. Assembly of Bimetallic PdAg Nanosheets and Their Enhanced Electrocatalytic Activity toward Ethanol Oxidation. *Langmuir* **2020**, *36*, 11094–11101. [[CrossRef](#)] [[PubMed](#)]
48. Fang, C.; Xu, X.; Zhao, J.; Cui, Z.; Yu, N.; Bi, T.; Hu, J.; Jiang, X. Composition and size engineering of porous PdAg alloy for high performance ethanol electrooxidation. *J. Alloys Compd.* **2019**, *806*, 239–245. [[CrossRef](#)]
49. Lv, H.; Wang, Y.; Lopes, A.; Xu, D.; Liu, B. Ultrathin PdAg single-crystalline nanowires enhance ethanol oxidation electrocatalysis. *Appl. Catal. B* **2019**, *249*, 116–125. [[CrossRef](#)]
50. Queiroz, M.A.R.; Ribeiro, J. Catalysts of PtSn/C Modified with Ru and Ta for Electrooxidation of Ethanol. *Catalysts* **2019**, *9*, 277. [[CrossRef](#)]
51. Cullity, B.D. *Elements of X-ray Diffraction*, 2nd ed.; Addison-Wesley Publishing Company: Boston, MA, USA, 1978. Available online: https://books.google.com.br/books/about/Elements_of_X_ray_Diffraction.html?id=WpxpAAAAMAAJ&redir_esc=y (accessed on 29 August 2021).
52. Grden, M.; Lukaszewski, M.; Jerkiewicz, G.; Czerwinski, A. Electrochemical behaviour of palladium electrode: Oxidation, electrodisolution and ionic adsorption. *Electrochim. Acta* **2008**, *53*, 7583–7598. [[CrossRef](#)]